# Effects of Products of Inertia on Re-Entry Vehicle Roll Behavior

ALBERT E. HODAPP JR.* AND EDWARD L. CLARK JR.*
*Sandia Laboratories, Albuquerque, N. Mex.*

**Ballistic re-entry vehicles having lateral center-of-gravity offsets (mass asymmetries) exhibit anomalous roll behavior as a result of trim-angle-generated lateral aerodynamic forces. The trim angles caused by mass and aerodynamic asymmetries have been thoroughly investigated. However, inertia asymmetries, which result when the principal axes of the vehicle become inclined with respect to the body reference axes, are a source of trim angle which has not been considered in detail. This paper presents a linear quasi-steady theory which demonstrates that inertia asymmetries are 1) more effective than equivalent mass and aerodynamic asymmetries in generating trim angles over the super-resonant region of re-entry flight; 2) equally as effective at resonance; and 3) less effective over the subresonant region. The predictions of the theory are verified by numerical integrations of the complete equations of motion and by the the results of three angular degree-of-freedom wind-tunnel experiments.**

## Nomenclature

c.g. = center of gravity
$C_A$ = axial force coefficient, axial force/$q'S$
$C_m$ = pitching moment coefficient, pitching moment/$q'Sd$
$C_{m_0}$ = pitching moment coefficient at $p = 0$ caused by aerodynamic asymmetries
$C_{m_q}$ = damping derivative coefficient, $\partial C_m/\partial(qd/2V)$, rad$^{-1}$
$C_{m_\alpha}$ = pitching moment slope coefficient, $\partial C_m/\partial\alpha$, rad$^{-1}$
$C_{m_{\dot\alpha}}$ = damping derivative coefficient, $\partial C_m/\partial(\dot\alpha d/2V)$, rad$^{-1}$
$C_{m_{p\beta}}$ = Magnus moment coefficient, $\partial^2 C_m/\partial(pd/2V)\partial\beta$, rad$^{-1}$
$C_N$ = normal force coefficient, normal force/$q'S$
$C_{N_\alpha}$ = normal force slope coefficient, $\partial C_N/\partial\alpha$, rad$^{-1}$
$C_n$ = yawing moment coefficient, yawing moment/$q'Sd$
$C_{n_0}$ = yawing moment coefficient at $p = 0$ caused by aerodynamic asymmetries
$d$ = vehicle base diameter (Fig. 1), ft
$F_T$ = trim force (Fig. 2), lb
$h$ = altitude, ft
$i$ = $(-1)^{1/2}$
$I, I_Y, I_Z$ = lateral moments of inertia, $I = I_Y = I_Z$, slug-ft$^2$
$I_X$ = axial moment of inertia, slug-ft$^2$
$J_{XY}, J_{YZ}, J_{XZ}$ = products of inertia, slug-ft$^2$
$m$ = vehicle mass, slugs
$M_X, M_Y, M_Z$ = aerodynamic moments about $X$, $Y$, $Z$ axes, respectively, lb-ft
$p,q,r$ = angular velocities about $X,Y,Z$ axes, respectively, rad/sec
$p_{cr}$ = critical roll rate [Eq. (5)], rad/sec
$q'$ = dynamic pressure, lb/ft$^2$
$S$ = reference area, $S = \pi d^2/4$, ft$^2$
$t$ = time, sec
$V$ = total velocity, fps
$X,Y,Z$ = body reference axes, mutually parallel to geometric axes, with origin at the c.g. (Fig. 1)
$X_g, Y_g, Z_g$ = geometric axes, with $X_g$ the axis of geometric symmetry (Fig. 1)
$X_p, Y_p, Z_p$ = principal axes (Fig. 1)
$y_{cg}, z_{cg}$ = position of the c.g. relative to origin of geometric axes along positive $Y_g$ and $Z_g$ axes, respectively (Fig. 1), ft
$\alpha$ = angle of attack, rad or deg
$\alpha_0, \beta_0$ = trim angles of attack and sideslip at $p = 0$ which result from aerodynamic asymmetries, rad or deg
$\beta$ = sideslip angle, rad or deg
$\gamma$ = flight path angle, deg
$\delta_\beta, \delta_\alpha$ = inclination angles between principal axes and body reference axes [Eq. (1) and Fig. 1], rad or deg
$\zeta$ = complex total angle of attack [Eq. (1)], rad or deg
$\lambda, \mu$ = roll rate and damping ratios [Eq. (5)]
$\rho$ = atmospheric density, slug/ft$^3$
$\phi$ = aerodynamic roll range (Fig. 2), rad or deg
$|\ |$ = absolute value or magnitude
$(\bar{\ })$ = complex quantity
$(\dot{\ }), (\ddot{\ })$ = first and second derivatives with respect to time

### *Subscripts*

$i, R, T$ = initial, reference, and trim conditions

## Introduction

A SLENDER ballistic re-entry vehicle that has a lateral center-of-gravity offset (mass asymmetry) may exhibit anomalous roll behavior as a result of the roll torque due to lateral aerodynamic force and the mass asymmetry. The aerodynamic force is caused by the total angle of attack, which consists of transient and trim components. Although conditions exist for which the transient component can cause sustained changes in roll rate,[1] the trim angle of attack is the cause of almost all cases of re-entry vehicle spinup and spin down due to lateral aerodynamic force. The trim angles of attack resulting from mass and/or aerodynamic asymmetries have been thoroughly investigated.[1-3] However, little is known about the trim angle resulting from an inertia asymmetry; i.e., an asymmetry resulting from products of inertia that cause the principal axes to be inclined with respect to the body reference axes. Nicolaides,[4] Vaughn,[5] and Carlson and Louis[6] all pointed out the existence of a trim angle due to this source. Glover[2] investigated the inertial rolling moments due to products of inertia; however, these moments are generally quite small compared with the trim-angle-induced moment. The behavior of the trim angle due to inertia asymmetry is described in detail in this paper. Comparisons are made

Presented as Paper 70-204 at the AIAA 8th Aerospace Sciences Meeting, New York, January 19-21, 1970; submitted May 18, 1970; revision received September 18, 1970. This work was supported by the U.S. Atomic Energy Commission.

* Member of the Technical Staff, Aerothermodynamics Projects Department. Member AIAA.

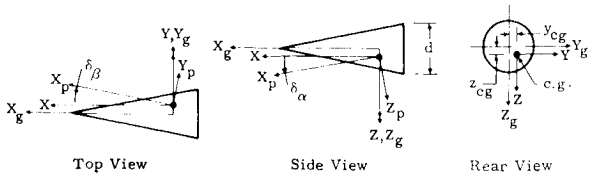


**Fig. 1 Coordinate systems and nomenclature.**

with the behavior of trim angles caused by mass and aerodynamic asymmetry. Both theoretical evidence and experimental evidence are presented that demonstrate that flight regions exist over which inertia asymmetries can cause trim angles as large as or larger than those resulting from equivalent mass and aerodynamic asymmetries; therefore, they can cause large continuous changes in roll rate when mass asymmetry is present.

The study[7] from which these results were obtained was conducted in three phases. First, a quasi-steady theory was developed to provide an insight into the behavior of the trim angle resulting from an inertia asymmetry. This theory also includes effects of mass and aerodynamic asymmetries. Second, six-degree-of-freedom (6-DOF) digital simulations were obtained to confirm the existence and severity of product-of-inertia-induced trim angles. Finally, experimental results were obtained and compared with the theory.

## Theoretical Analysis

### Equations of Angular Motion

The complex differential equation of angular motion relative to body-fixed axes $X,Y,Z$ (Fig. 1), which includes effects of mass, aerodynamic, and inertia asymmetries, may be written as

$$\ddot{\bar{\zeta}} + \bar{A}\dot{\bar{\zeta}} + \bar{B}\bar{\zeta} = \bar{C} \tag{1}$$

where

$$\bar{\zeta} = \beta + i\alpha$$

$$\bar{A} = -\left[\frac{q'S}{mV}(C_A - C_{N\alpha}) + \frac{q'Sd^2}{2VI}(C_{m_q} + C_{m_{\dot{\alpha}}}) - ip\left(2 - \frac{I_X}{I}\right)\right]$$

$$\bar{B} = -\left\{\frac{q'Sd}{I}C_{m_\alpha} + p^2\left(1 - \frac{I_X}{I}\right) + ip\frac{q'S}{V}\left[\frac{1}{m}\left(1 - \frac{I_X}{I}\right)(C_A - C_{N\alpha}) + \frac{d^2}{2I}(C_{m_q} + C_{m_{\dot{\beta}}})\right]\right\}$$

$$\bar{C} = -p^2\left(1 - \frac{I_X}{I}\right)(\delta_\beta + i\delta_\alpha) + i\frac{q'Sd}{I} \times \left\{\left[C_{m_0} + C_A\left(\frac{z_{cg}}{d}\right)\right] + i\left[C_{n_0} - C_A\left(\frac{y_{cg}}{d}\right)\right]\right\}$$

$$\delta_\beta \simeq J_{XY}/(I - I_X) \qquad \delta_\alpha \simeq J_{XZ}/(I - I_X)$$

This equation was derived by the authors[7] on the basis of the following assumptions: a) The vehicle experiences only small angular perturbations ($\alpha$ and $\beta \ll 1$ rad); b) the moment-of-inertia tensor is symmetric with $I = I_Y = I_Z$; $J_{YZ} = 0$; and $J_{XY}$ and $J_{XZ} \ll I$; c) the vehicle has linear aerodynamics and retains basic aerodynamic symmetry; therefore, mass and aerodynamic asymmetries are small ($y_{cg}/d$ and $z_{cg}/d \ll 1$; $C_{m_0}/C_{m_\alpha}$ and $C_{n_0}/C_{m_\alpha} \ll 1$); d) the effects of gravity are negligible. The forcing function $\bar{C}$ in Eq. (1), contains the parameters which cause the vehicle to trim at an attitude angle other than zero. Contributors to the total trim angle of attack are mass asymmetries $y_{cg}$ and $z_{cg}$, aerodynamic asymmetries $C_{m_0}$ and $C_{n_0}$, and inertia asymmetries $\delta_\beta$ and $\delta_\alpha$.

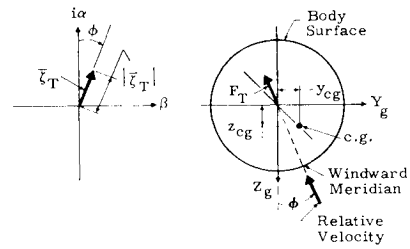


**Fig. 2 Orientation of total trim angle, trim force, and windward meridian.**

The $\bar{C}$ term in Eq. (1) is separated into two distinct groups of parameters. The group that results from inertia asymmetry is multiplied by roll rate squared; the group that results from mass and aerodynamic asymmetry is multiplied by $q'Sd/I$. This grouping of parameters indicates that the trim angles that result from mass and aerodynamic asymmetries will display similar behavior, whereas the inertia asymmetry-induced trim angle will display a distinctly different behavior.

Equation (1) is a linear differential equation with variable coefficients. In order to simplify both the task of solving this equation and the algebraic form of its solution, it was assumed that the coefficients $\bar{A}$, $\bar{B}$, and $\bar{C}$ can be considered constant over small time intervals. Since only the trim angle of attack is of interest in this study, the additional restriction of negligible transient angle of attack was imposed. Therefore, the solution of Eq. (1) reduces to the particular solution which is given as

$$\bar{\zeta}_T = \bar{C}/\bar{B} \tag{2}$$

where $\bar{\zeta}_T$ is the complex total trim angle of attack. By the restrictions imposed, it is also the total angle of attack.

A consequence of assuming $\bar{A}$, $\bar{B}$, and $\bar{C}$ to be constant is that Eq. (2) will always predict the steady-state trim angle of attack at each instant of time. During re-entry, the trim angle does not respond instantaneously, and in some cases may never reach the steady-state value. These differences in the theoretically predicted trim and the actual trim are usually small but become apparent when the vehicle is passing through high-altitude resonance (first resonance†).

The assumption of negligibly small transient angle of attack is not overly restrictive, since many trajectories of interest involve small initial transients that damp rapidly. It is often observed in 6-DOF digital simulations[1,2,8] that even where large initial transient angles of attack exist, soon after occurrence of first resonance the total angle of attack damps to the trim angle, and the vehicle flies over a large portion of the re-entry trajectory in lunar motion.

### Trim Angle of Attack

Two approaches can be taken to study the behavior of $\bar{\zeta}_T$. The first is to separate Eq. (2) into two components and develop separate expressions for the trim angle due to inertia asymmetry, and for the trim angle due to mass and aerodynamic asymmetry. The development of the expressions for these trim angle components has been given elsewhere.[7,9] The second approach, for which results will be presented, is to develop an expression for the trim angle which contains the combined effects of inertia, mass, and aerodynamic asymmetries.[7,9] The trim angle component expressions are useful for studying the details of trim angle behavior, while the trim angle expression that includes combined effects is more satisfactory for determining re-entry vehicle roll behavior.

As shown in Fig. 2, the complex total trim angle of attack $\bar{\zeta}_T$ can be described by its magnitude $|\bar{\zeta}_T|$ and orientation

† First resonance is the initial crossing of the vehicle's roll rate and its undamped natural frequency.

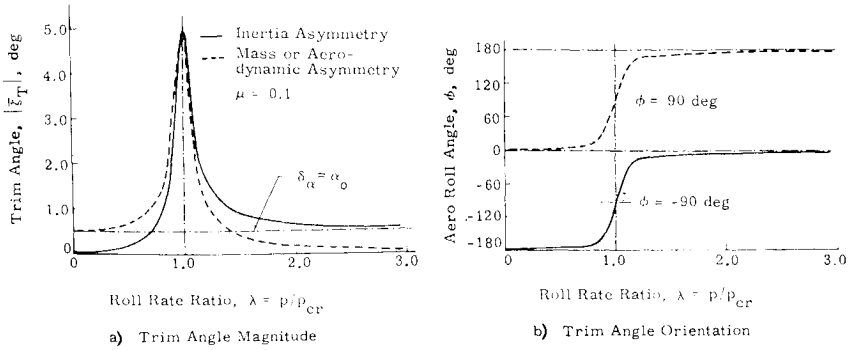


**Fig. 3 Trim angle response.**

angle $\phi$, as follows: $\bar{\xi}_T = \beta_T + i\alpha_T = |\bar{\xi}_T|\ (\sin\phi + i\cos\phi)$. The aerodynamic roll angle $\phi$ gives the position of the windward body meridian and the orientation of $F_T$, the transverse component of trim force.

The trim angle magnitude is

$$|\bar{\xi}_T| = \left[\frac{(\beta_{T_R} - \lambda^2\delta_\beta)^2 + (\alpha_{T_R} - \lambda^2\delta_\alpha)^2}{(1-\lambda^2)^2 + (\mu\lambda)^2}\right]^{1/2} \tag{3}$$

and the orientation of the trim angle is

$$\phi = \tan^{-1}[(\beta_{T_R} - \lambda^2\delta_\beta)/(\alpha_{T_R} - \lambda^2\delta_\alpha)] + \tan^{-1}[\mu\lambda/(1-\lambda^2)] \tag{4}$$

where $\alpha_{T_R}$ and $\beta_{T_R}$ are the reference trim angles which result from mass and aerodynamic asymmetries; $\delta_\alpha$ and $\delta_\beta$ are the reference trim angles which result from inertia asymmetry; and‡

$$\lambda = p/p_{cr} \qquad p_{cr} = \pm[-C_{m_\alpha} q' Sd/(I - I_X)]^{1/2}$$

$$\mu = \pm\left\{-\rho^{1/2}S\left[\frac{1}{2m}(C_A - C_{N_\alpha}) + \frac{d^2}{4}\left(\frac{C_{m_q} + C_{m_{\dot\beta}}}{I - I_X}\right)\right]\Big/\left[\frac{-C_{m_\alpha}Sd}{2(I-I_X)}\right]^{1/2}\right\} \tag{5}$$

At resonance ($\lambda = 1$), the undamped natural frequency of vehicle motion is equal to $p_{cr}$, the critical roll rate.

The sign of $p_{cr}$ is always the same as that of $p$; therefore, the roll-rate ratio $\lambda$ is always positive. Similarly, the sign outside the brackets in the expression for the damping ratio $\mu$ is the same as that of $p$. In most cases of interest, the aerodynamic coefficients combine to yield a positive term within the brackets; then, $\mu$ has the sign of the roll rate. However, it is possible that the aerodynamic coefficients can cause $\mu$ to have the opposite sign.

The condition $p = 0$ is chosen as the reference condition for mass and aerodynamic asymmetry-induced trim angle. At $p = 0$, $\bar{\xi}_T = (\beta_{T_R} + i\alpha_{T_R})$ where

$$\alpha_{T_R} = \alpha_0 - C_A\, z_{cg}/C_{m_\alpha} d$$

and

$$\beta_{T_R} = \beta_0 - C_A\, y_{cg}/C_{m_\alpha} d$$

The quantities $\alpha_0$ and $\beta_0$ are the nonrolling angle of attack and sideslip angle caused by aerodynamic asymmetries, $\alpha_0 = -C_{m_0}/C_{m_\alpha}$ and $\beta_0 = C_{n_0}/C_{m_\alpha}$.

For inertia asymmetry-induced trim angle, it is desirable to use $p \to \infty$ as a reference condition. As $p \to \infty$, $\bar{\xi}_T \to (\delta_\beta + i\delta_\alpha)$, where the reference trim angles $\delta_\beta$ and $\delta_\alpha$ are defined in terms of moments and products of inertia in Eq. (1).

### Trim Angle Behavior

Equations (3) and (4) show that the total trim angle is a function of the reference quantities and the parameters $\mu$ and $\lambda$. The trim angle magnitude and orientation are primarily functions of the roll-rate ratio $\lambda$; however, the damping ratio $\mu$ also is important because it limits the trim angle magnitude and controls the region around resonance ($\lambda = 1$) over which significant changes in $\phi$ can occur. Since $\mu$ is usually very small, large changes in trim angle orientation $\phi$ occur very close to resonance. Equation (5) shows that $\mu$ is directly proportional to $\rho^{1/2}$; hence, $\mu$ increases with decreasing altitude. Thus, as altitude decreases, the trim angle-of-attack magnitude at resonance decreases,[1] and the region around resonance over which significant changes in $\phi$ occur increases.

The different behavior patterns of trim angles due to inertia asymmetries and those due to aerodynamic asymmetries can be illustrated by use of Eqs. (3) and (4). Figure 3 shows a trim-angle-behavior comparison for two vehicles identical in every detail except for their asymmetries. One has only an inertia asymmetry ($\delta_\alpha$) and the other has only an aerodynamic asymmetry ($\alpha_0$). Both reference trim angles ($\delta_\alpha$ and $\alpha_0$) are positive and have a magnitude of 0.5°. The aerodynamic asymmetry could have been replaced by an equivalent mass asymmetry ($z_{cg}/d = -C_{m_\alpha}\alpha_0/C_A$) to obtain identical trim-angle behavior; thus, the term "mass or aerodynamic asymmetry" is used in Fig. 3.

Figure 3a shows that at resonance ($\lambda = 1$) the trim angles that result from these equivalent asymmetries are equal. However, they are equal only at resonance; above and below resonance they display opposite trends. When the roll rate is super-resonant ($\lambda > 1$), the inertia asymmetry-induced trim angle is never smaller than the principal axis inclination angle $\delta_\alpha$, whereas the trim angle induced by mass or aerodynamic asymmetries approaches zero. Conversely, when the roll rate is subresonant ($\lambda < 1$), the mass or aerodynamic asymmetry-induced trim angle is never smaller than the nonrolling reference value, whereas the inertia asymmetry-induced trim angle approaches zero. At zero roll rate, the trim angle due to inertia asymmetry is zero.

Figure 3b shows that for equal reference quantities the angular positions $\phi$ of the two types of trim angle differ by a constant 180°. This means that the trim angles undergo identical changes in position as the roll-rate ratio $\lambda$ changes. For both types of trim angle, the trim angle position $\phi$ changes in a positive sense as the roll rate increases positively from $p = 0$ (Fig. 2). The 180° change in trim angle position as the roll rate is varied from $p = 0$ through resonance to $p \to \infty$, and the 90° change in position in going from a reference roll-rate condition to resonance, are both characteristics of second-order linear systems.

### External Roll Torque

The external roll torque $M_X$, which results from mass asymmetry and lateral trim force, is a primary cause of the anomalous roll behavior exhibited by slender ballistic re-entry vehicles. Lateral trim forces can be resolved into components in the plane (in-plane) defined by the c.g. and the $X_g$ axis (Fig. 2), and into components perpendicular to this plane (out-of-plane). The out-of-plane component generates the external roll torque. Since the roll-rate ratio $\lambda$ must change

‡ The damping ratio $\mu$ as defined in Eq. (5) is twice the value used by Pettus[1] and Barbera.[3]

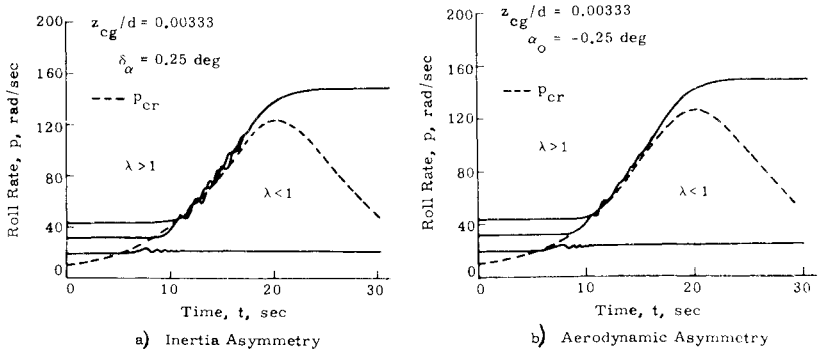


**Fig. 4 Roll histories for equivalent in-plane asymmetries.**

during re-entry, the aerodynamic roll angle or trim angle position, $\phi$, must also change (Fig. 3b); therefore, any trim force will develop an out-of-plane component, regardless of its reference position.

Asymmetries are designated in-plane or out-of-plane depending on the position of the trim force in the body at the reference roll-rate condition. The torques generated by in-plane and out-of-plane asymmetries display distinctly different behavior as the roll rate changes from the reference condition and proceeds through resonance to the other roll-rate extreme. The characteristic behavior of these torques was given by Barbera[3] for mass and aerodynamic asymmetries and by the authors[7,9] for inertia asymmetries.

### Equation of Rolling Motion

The assumptions listed after Eq. (1) were used to reduce the six equations of rigid body motion to three equations. Two of these equations were combined to form Eq. (1) and the third equation, the equation of rolling motion, is given below.

$$\dot{p} = (1/I_X)\{+ (1M_X/I)[J_{XY}(M_Y - I_X pr) + J_{XZ}(M_Z + I_X pq)]\} \quad (6)$$

where

$$M_X = q'Sd[C_{N\alpha}\alpha_T(y_{cg}/d) - C_{N\alpha}\beta_T(z_{cg}/d)]$$

$$M_Y = q'Sd[-C_{m_\alpha}(\alpha_{TR} - \alpha_T) + C_{m_q}(qd/2V) + C_{m_{\dot\beta}}(pd/2V)\beta_T]$$

$$M_Z = q'Sd[C_{m_\alpha}(\beta_{TR} - \beta_T) + C_{m_q}(rd/2V) + C_{m_{\dot\beta}}(pd/2V)\alpha_T]$$

$$\alpha_T = |\bar{\xi}_T| \cos\phi, \qquad \beta_T = |\bar{\xi}_T| \sin\phi$$

$$q = p\beta_T - q'S(C_A - C_{N\alpha})\alpha_T/mV$$

$$r = p\alpha_T + q'S(C_A - C_{N\alpha})\beta_T/mV$$

The second term on the right side of Eq. (6) must be considered when products of inertia are present. These inertial roll torques are almost always small compared with the external roll torque, $M_X$; however, conditions do exist along a re-entry trajectory where the inertial torques can be as large as or larger than $M_X$. Pure roll torques and roll-damping torques have been neglected in Eq. (6).

Unfortunately, Eq. (6) cannot be solved in closed form to obtain the roll rate $p$. However, when the trajectory parameters $q'$ and $V$ are available, the roll rate can be determined by numerical integration of the equation.

## Numerical Integrations

The preceding theoretical development yields an analytical tool whereby a more complete knowledge of trim angle behavior can be gained for slender ballistic re-entry vehicles. The quasi-steady theory predicts that inertia asymmetries are 1) more effective than equivalent mass and aerodynamic asymmetries§ in generating trim angles over the super-resonant region of re-entry flight; 2) equally as effective at resonance; and 3) less effective over the subresonant region (Fig. 3). These predictions will be verified by comparing roll-rate histories obtained by numerically integrating the complete 6-DOF equations of rigid-body motion. For the comparisons shown in Figs. 4 and 5, the re-entry conditions and all vehicle parameters were identical, except for the aerodynamic and inertia asymmetries.

The mass asymmetry required to produce the external roll torque $M_X$ was held at a fixed value in the comparisons ($z_{cg}/d = 0.00333$); therefore, any differences in the roll-rate histories can be attributed to differences in the trim angles of attack due to aerodynamic and inertia asymmetries. Mass asymmetry, independent of other asymmetries, always produces a roll torque that tends to decrease the absolute magnitude of the roll rate. Because of its inherent in-plane reference position, it has a negligible effect on the roll rate except for conditions very close to resonance. The mass asymmetry being considered in Figs. 4 and 5 is relatively large, yet it produces a hypersonic reference trim angle $\alpha_{TR}$ of 0.04°, which is small compared to the reference trim angles (0.25°) being considered for the inertia and aerodynamic asymmetries. This particular mass asymmetry would cause less than a 1.8 rad/sec reduction in roll rate at first resonance for the re-entry conditions and initial roll rates used for Figs. 4 and 5; however, near second resonance it could cause a large change in roll rate.

The configuration used for these re-entry simulations was the Sandia Re-Entry Vehicle Resonance Test Vehicle (RVRTV), a 10° half-angle cone having a 1.25-ft base diameter, a nose-to-base radius ratio of 0.0167, and a 6% hypersonic static margin. The external geometry of this vehicle is the same as the standard dynamic stability calibration model used by the Supersonic Tunnel Association and the AGARD.[10]

The initial re-entry conditions used for the 6-DOF digital simulations were $V_i$ = 21,600 fps, $\gamma_i$ = −20.6°, and $h_i$ = 180,000 ft. All angular motion parameters except the roll rate were initially set to zero. This resulted in small initial transient angles of attack in the 6-DOF simulations, since the vehicle had a trim angle. Three initial values of roll rate were used in these simulations to emphasize the large effect that initial roll rate can have on the roll-rate histories.

Re-entry trajectories are influenced by the angle-of-attack magnitude, which, in turn, depends somewhat on the vehicle's roll-rate history. The trajectories from which the roll-rate histories of Figs. 4 and 5 were obtained are appreciably different in some cases because the three initial values of roll rate result in different angle-of-attack histories. To avoid confusion in these figures, the critical roll-rate histories, which are trajectory dependent, are presented only for those cases where large changes in roll rate occur.

§ That is, mass and aerodynamic asymmetries having reference magnitudes equal to the reference magnitude of the inertia asymmetry.

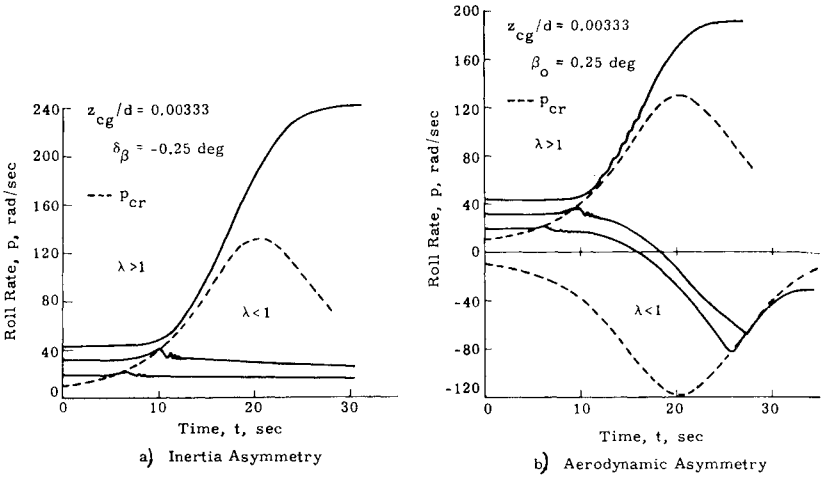


**Fig. 5 Roll histories for equivalent out-of-plane asymmetries.**

In Fig. 4, the reference orientation of the trim angles caused by the inertia and aerodynamic asymmetries are in-plane, but differ in position by 180°. This 180° difference in the reference trim orientations causes the trim angles to occupy identical positions $\phi$ in their respective bodies as the roll-rate ratio $\lambda$ changes. The reference magnitudes of these trim angles are equal. This figure shows that near resonance ($\lambda = 1$) the trim angles that result from these inertia and aerodynamic asymmetries produce equivalent changes in roll rate. The trim angles must be equivalent (Fig. 3a), since the mass asymmetry of each body is the same. In these over-spin cases the roll rate ceases to increase as it moves deeper into the super-resonant region ($\lambda > 1$), because at conditions away from resonance the trim force moves back in-plane where it can no longer generate a roll torque. For similar reasons, no appreciable change in roll rate was observed for those roll histories in the subresonant region ($\lambda < 1$).

Figure 5 compares the changes in roll rate caused by out-of-plane trim angles that result from inertia and aerodynamic asymmetries. The reference trim angles have equal magnitudes and are orientated in the body (180° apart) to generate a positive roll torque in the super-resonant region. These results establish that the inertia asymmetry generates a larger trim angle in the super-resonant region, since it causes the greatest change in the roll rate. The reason for this is that the trim angle resulting from the inertia asymmetry is never smaller than its reference value in this region, while the trim angle due to the aerodynamic asymmetry goes to zero (Fig. 3a). The increase in roll rate produced by the inertia asymmetry in this region is terminated only by the decreasing dynamic pressure.

At the two lower values of initial roll rate (Fig. 5), both types of asymmetries cause their respective vehicles to spin up ahead of first resonance, then break through and spin down in the subresonant region. The trim angle produced by the inertia asymmetry approaches zero in this region, and is zero at zero roll rate (Fig. 3a). Therefore, as shown in the figure, the inertia asymmetry is not as effective as the aerodynamic asymmetry in this region, and cannot cause the vehicle to spin through zero ($p = 0$). The trim angle that results from aerodynamic asymmetry is never smaller than the reference value in the subresonant region, and takes on the reference value at zero roll rate (Fig. 3a). Therefore, as shown in Fig. 5b, the aerodynamic asymmetry can cause the vehicle to spin through zero and is more effective throughout the entire subresonant region.

Comparison of the results in Fig. 4 with those in Fig. 5 shows that the in-plane orientation of the trim angle displays the greatest tendency to produce over-spin near first resonance;[3] i.e., with equivalent asymmetry magnitudes, over-spin occurs at a lower initial roll rate. The 6-DOF digital simulations presented here and those presented previously[7,9] all verify the trends predicted by the quasi-steady theory. Although the principal value of this theory lies in its ability to predict trends, it can also be used to predict the roll-rate magnitude very accurately when the assumptions of the theory are satisfied. In Figs. 6 and 7, comparisons are given between roll histories predicted by the quasi-steady theory and those predicted by 6-DOF simulations. The theoretical predictions were obtained by incorporating the quasi-steady theory [Eqs. (3) and (4)] into a point mass trajectory program.[7] Using the trim angle and trajectory information provided by the program, Eq. (6) is integrated numerically to obtain the roll-rate history. Two extreme examples were chosen for comparison, an over-spin caused by inertia asymmetry, and a spin through zero to lock-in for an aerodynamic asymmetry. As shown in these figures, excellent agreement is obtained in these cases where the assumptions of the theory are satisfied.

Situations have been observed at or near first resonance where the 6-DOF results predict an uneventful passage of the roll rate through first resonance, while the quasi-steady theory predicts large continuous changes in roll rate. This disagreement occurs because the actual trim angle buildup lags the theoretically predicted buildup, and may never reach the large steady-state value of trim angle predicted by the theory during the brief passage through first resonance. In these situations, the large trim magnification ratios at first resonance cause the theory to predict angles that far exceed the restrictions on the theory. At low altitudes, agreement

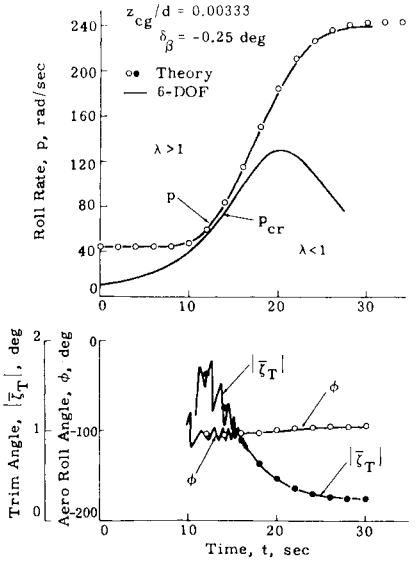


**Fig. 6 Comparison of theory with 6-DOF results for an inertia asymmetry.**

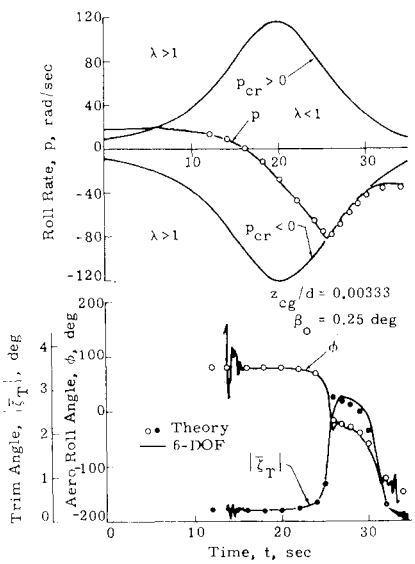


**Fig. 7 Comparison of theory with 6-DOF results for an aerodynamic asymmetry.**

between theory and 6-DOF near second resonance similar to that shown in Fig. 7 is typical, since the magnification ratio and the angle of attack transients are usually small at this condition.

## Experimental Results

To verify the quasi-steady theory further, a wind-tunnel dynamic stability test was conducted with a model that had mass and inertia asymmetries. The test configuration was a two-thirds scale model of the RVRTV previously described. The c.g. was located at 55% of the body length (14% static margin), and was offset from the model geometric centerline by 0.1 in. along the $Z_g$ axis (Fig. 1). Initially, the model was dynamically balanced to insure that the principal axes were parallel with the geometric axes. An inertia asymmetry was then introduced by adding weights to produce an out-of-plane principal inclination of 0.53°. The weights were designed to maintain static balance about the c.g. and to keep the lateral moments of inertia equal.

A sting-supported balance,[11] which incorporates a spherical gas bearing as the pivot, was used to support the model, thereby allowing it to have three angular degrees of freedom with negligible pivot friction. The model was unrestrained in roll, but was limited to a 10° total angle of attack. The test was conducted at the Arnold Engineering Development Center (AEDC) in the 50-in.-diam hypersonic tunnel B at a Mach number of 8, and a Reynolds number of $2.9 \times 10^6$ based on model length.

The model was tested at four initial values of roll rate, which were selected to cover the full spectrum of roll behavior; i.e., sub- and super-resonant conditions at positive and negative initial values of roll rate. Three runs were made at each initial roll rate, and repeatability of the data was excellent. The results of the experiment are presented in Fig. 8, where the plotted points are average values from the three runs. The subresonant and super-resonant regions in Fig. 8a appear different from those in the flight simulations because the dynamic pressure is constant in the wind tunnel; therefore, the critical roll rate curves are constant with time. Agreement between predictions of the quasi-steady theory and experimental results is excellent. The experimental data confirm that inertia asymmetries are much more effective in the super-resonant region.

The transient angle of attack was negligible for the subresonant spinup case, and the trim angle could be measured easily throughout the run. Results of these measurements are presented in Fig. 8b. Comparison of the experimental and theoretical results for the trim angle shows that the agreement is very good up to a roll-rate ratio of about 0.9. At higher values of the roll-rate ratio, the characteristic lead of the quasi-steady theory is evident. As shown, this discrepancy has a negligible effect on the roll histories.

Transient angles of attack were present throughout the super-resonant measurements. The effect of transient angle of attack was investigated by numerically integrating the complete equations of motion for a rigid body having three angular degrees of freedom. Excellent agreement was obtained when the results of these integrations were compared with the quasi-steady predictions and experimental results. This indicates that the lightly damped transient angle of attack observed in the super-resonant cases had a negligible effect on the roll histories.

## Conclusion

Results presented in this paper indicate that the effects of inertia asymmetries on the performance of ballistic re-entry vehicles should not be neglected. Specific conclusions that can be drawn from these results are as follows: 1) When the principal axes and the reference axes of a rolling vehicle become angularly misaligned, a trim angle of attack results. 2) These inertia-induced trim angles a) are never smaller than the principal axis inclination angle in the super-resonant region of re-entry flight; b) undergo a magnification at resonance equal to that experienced by trim angles induced by mass and aerodynamic asymmetries; c) may be smaller than the principal axis inclination angle in the subresonant region;

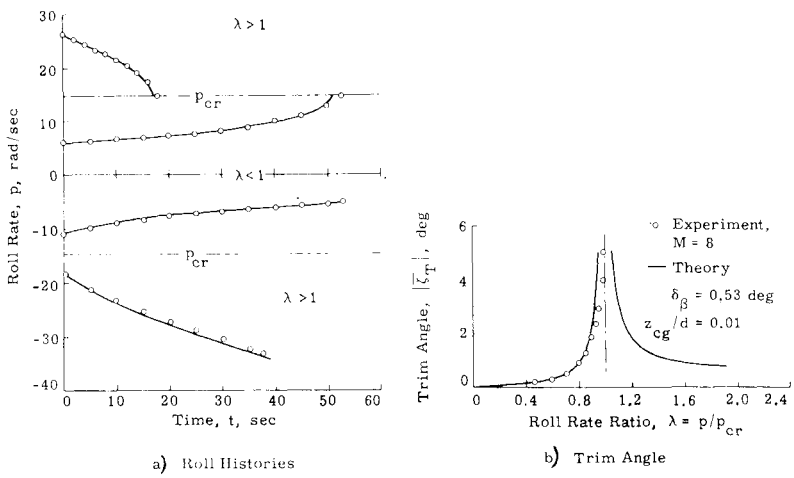


**Fig. 8 Comparison of theory with experimental results for an inertia asymmetry.**

and d) are zero at roll rate. 3) Small trim angles of attack ($\bar{\zeta}_T \leq 0.25°$), which can be produced by principal axis inclination angles of similar magnitude, may seriously degrade the performance of re-entry vehicles that have mass asymmetries. 4) Effects of inertia asymmetries on the angular and rolling motions of ballistic re-entry vehicles may be misinterpreted as the effects of mass and aerodynamic asymmetries.

## References


[1] Pettus, J. J., "Persistent Re-Entry Vehicle Roll Resonance," AIAA Paper 66-49, New York, Jan. 1966.

[2] Glover, L. S., "Effects on Roll Rate of Mass and Aerodynamic Asymmetries for Ballistic Re-Entry Bodies," *Journal of Spacecraft and Rockets*, Vol. 2, No. 2, March–April 1965, pp. 220–225.

[3] Barbera, F. J., "An Analytical Technique for Studying the Anomalous Roll Behavior of Re-Entry Vehicles," *Journal of Spacecraft and Rockets*, Vol. 6, No. 11, Nov. 1969, pp. 1279–1284.

[4] Nicolaides, J. D., "Missile Flight and Astrodynamics," TN 100A, 1959–61, U.S. Bureau of Weapons, Dept. of the Navy, Washington, D.C.

[5] Vaughn, H. R., "Boundary Conditions for Persistent Roll Resonance on Re-Entry Vehicles," SC-RR-67-287, May 1967, Sandia Labs., Albuquerque, N. Mex.

[6] Carlson, R. W. and Louis, C. A., III, "Introduction to Re-Entry Flight Dynamics," LMSC-D050690, March 1968, Lockheed Missiles & Space Co., Sunnyvale, Calif.

[7] Hodapp, A. E., Jr. and Clark, E. L., Jr., "A Technique for Determining Approximate Roll Rate Histories for Ballistic Re-entry Vehicles Having Mass, Inertia, and Aerodynamic Asymmetries," SC-RR-69-804, Sept. 1970, Sandia Labs., Albuquerque, N. Mex.

[8] Platus, D. M., "A Simple Analysis of Re-Entry Vehicle Roll Resonance," TR-1001(2240-30)-10, Jan. 1967, Aerospace Corp., El Segundo, Calif.

[9] Hodapp, A. E., Jr. and Clark, E. L., Jr., "The Effects of Products of Inertia on the Roll Behavior of Ballistic Re-Entry Vehicles," AIAA Paper 70-204, New York, Jan. 1970.

[10] Fail, R. and Garner, H. C., "Calibration Models for Dynamic Stability Tests," Rept. 563, 1968, Advisory Group for Aerospace Research and Development, Neuilly-sur-Seine, France.

[11] Ward, L. K., Jr. and Hodapp, A. E., Jr., "A Three-Degree-of-Freedom Dynamic Stability Balance for Use in the VKF Continuous Flow Hypersonic Tunnels ($M_\infty = 6$ through 12)," AEDC-TR-68-62, May 1968, Arnold Air Force Station, Tenn.


FEBRUARY 1971 J. SPACECRAFT VOL. 8, NO. 2

# An Exploratory Study of the Roll Behavior of Ablating Cones

JOHN B. MCDEVITT*
*NASA Ames Research Center, Moffett Field, Calif.*

**The coupling between roll dynamics and ablation patterns on cones has been investigated in the NASA Ames 3.5-Foot Hypersonic Wind Tunnel. A gas-bearing apparatus, which allowed the test models to be free in roll, was used to obtain the roll characteristics of a series of models exhibiting various ablation patterns (a basically subliming ablator and one involving a melt layer were used). Streamwise vortex grooving, turbulent wedge erosion, and cross-hatching were obtained by choosing suitable combinations of cone vertex angle and ablation material, and it was found that any of these patterns can introduce roll torques. For a subliming ablator, the direction of initial spin did not appear to bias the results, and reversals in torque direction were common. For a melting ablator it was found that torque in the direction of spin can also occur for the smooth cone if the model is rolling at angle of attack.**

## Nomenclature

$A_b,d$ = model base area and diameter
$C_l$ = rolling moment coefficient, $L/q_\infty A_b d$
$C_{lp}$ = roll damping derivative, $\partial C_l/\partial(pr_b/U_\infty)$
$h_0,h_1,n$ = shape change parameters, Eq. (A2)
$I_x$ = moment of inertia about cone axis
$K_{\text{tare}},K_{\text{aero}}$ = constants, Eqs. (1) and (2)
$L$ = rolling moment
$l$ = cone length
$M_\infty$ = freestream Mach number
$m/\rho_\infty U_\infty A_b$ = normalized ablation rate, ($\rho_\infty$ = freestream density)
$P,P_{t_1}$ = static and total pressures, respectively
$p,\varphi$ = roll rate, rad/sec
$\dot{p},\ddot{\varphi}$ = roll acceleration, rad/sec$^2$
$q_\infty$ = freestream dynamic pressure
$r_b$ = base radius of cone
$T_t$ = total temperature
$t$ = time
$U_\infty$ = freestream velocity
$W$ = weight of model
$x$ = axial distance from cone apex
$y,z,\theta$ = cylindrical coordinate system, Fig. 15
$\bar{y},\bar{z}$ = coordinates of the center of gravity for an ablating model
$\alpha,\beta$ = angles of attack and sideslip, respectively
$\lambda$ = angle between crossflow velocity vector and horizontal plane of tunnel, Fig. 15
$\sigma_c,\theta$ = cone semivertex and azimuthal angles, respectively
$\varphi$ = roll angle
$(\ )_0$ = at $p = 0$ or $t = 0$
$(\ )_\infty$ = freestream condition

Presented as Paper 70-562 at the AIAA Atmospheric Flight Mechanics Conference, Tullahoma, Tenn., May 13–15, 1970; submitted May 25, 1970; revision received October 22, 1970.

* Research Scientist. Member AIAA.

## Introduction

WILLIAMS[1] demonstrated that roll torques can develop for ablating cones, but his study was confined to static measurements using a strain-gage, flexural-pivot balance. The present paper describes a study wherein a gas-bearing apparatus, which allowed the test models to be free in roll, was used to obtain the roll characteristics of a series of models as they developed various ablation patterns that are identifiable with certain ablation-flow interaction phenomena.